Conformers of *n*-Si_5Me_{12}: A Comparison of ab Initio and Molecular Mechanics Methods

Bo Albinsson[1a]

Department of Physical Chemistry, Chalmers University of Technology, S-412 96 Göteborg, Sweden

Dean Antic,[1b] **Frank Neumann,**[1b] **and Josef Michl*,**[1b]

Department of Chemistry and Biochemistry, University of Colorado, Boulder, Colorado 80309-0215

Received: July 8, 1998; In Final Form: October 7, 1998

Optimized geometries of the conformers of permethylated linear pentasilane, *n*-Si_5Me_{12}, were calculated by the HF/3-21G*, MM3, MM2, and MM+ methods, which predict eight, nine, six, and six energetically distinct enantiomeric conformer pairs, respectively, at geometries representing various combinations of the anti (∼165°), ortho (∼90°), and gauche (∼55°) SiSiSiSi dihedral angles in the backbone. The results of the MM2 and MM+ methods, based on the same force field, differ insignificantly. The barriers between conformers appear to be exaggerated by the molecular mechanics methods, particularly MM2. Contour maps showing the ground-state energy as a function of the full range of two backbone SiSiSiSi dihedral angles, with all other geometrical variables optimized, computed by each of the methods (only a limited range of angles near the anti,anti geometry in the case of HF/3-21G*) are compared with each other and with analogous results for a model compound, Si_4Me_{10}. Conformer interconversion paths are discussed, and two meso transition states for enantiomer interconversion have been located at the HF/3-21G* level of calculation. At the eight HF/3-21G* optimized geometries, single-point energies (HF/6-31G* and MP2/6-31G*) and vibrational frequencies (HF/3-21G*) were computed. The predicted IR and Raman spectra suggest that about half of the expected conformers will be identifiable by vibrational spectroscopy under conditions of matrix isolation. Relative conformer energies calculated by the MM2 and HF methods are similar and favor the anti dihedral angles over gauche and ortho, in agreement with results of solution experiments. Those calculated by the MM3 and MP2 methods are similar to each other and favor both anti and gauche dihedral angles nearly equally over ortho, in agreement with indications provided by gas-phase experiments. A rationalization of these solvent effects is proposed. The energies of the conformers of Si_4Me_{10} and Si_5Me_{12} were used to set up a system of additive increments at the MM2, MM3, HF/3-21G*, HF/6-31G*, and MP2/6-31G* levels of calculation, which can be used to predict conformational energies of longer permethylated oligosilanes. An intrinsic energy value is assigned to each of the a, o, and g dihedral angles, and interaction energy values are assigned to each combination of two dihedral angles. The interaction values follow the expected rules in that equal twist sense is favored for adjacent aa, ag, oo, and gg pairs, whereas opposite twist sense is generally favored for adjacent ao and go pairs. The MM3-derived set of increments has been tested against results computed for Si_6Me_{14} and found to perform well.

Introduction

Oligosilanes, *n*-Si_nR_{2n+2} ($n \lesssim 20-30$), and polysilanes, *n*-Si_nR_{2n+2} ($n \gtrsim 20-30$), contain linear chains of silicon atoms (R need not be all identical).[2] Their unusual electronic properties display strong effects of σ conjugation.[3] The surprisingly long near-UV wavelength of the electronic absorption and emission peaks is primarily due to the properties of the backbone rather than the lateral substituents and has been attributed to the electropositive nature of silicon relative to carbon.[4] Striking thermochromism,[5] solvatochromism,[6] ionochromism,[7] piezochromism,[8] electrochromism,[9] and related properties of variously substituted polysilanes demonstrate that their electronic structure is strongly affected by chain conformation.[10] This is the case even in the shortest oligosilanes with more than one backbone conformer, *n*-Si_4H_{10}[11] and *n*-Si_4Me_{10}.[12]

Theoretical work has concentrated on infinite polymer chains using band structure methods[13] and on relatively short oligomers using molecular mechanics (MM) and molecular orbital (MO) methods. Numerous computational studies of the conformations of the neutral molecules[14−16] and their radical ions[17] and much electronic structure work have been reported. The simplest (Sandorfy C[18]) model of σ conjugation does not predict conformational dependence for UV absorption and emission, but the next more complicated (ladder C[19]) model, all-valence semiempirical methods,[20,21] and ab initio methods[11,12,22,23] all do. The latter methods suggest that the lateral substituents actually play a significant role in the excitation process in at least some of the conformations, making it unlikely that the simplest models of the C type,[18,19] which consider only the backbone, will be satisfactory. Despite much past effort, it is still impossible to predict the relative stabilities of the conformational forms from the knowledge of the substitution patterns, or to predict their electronic absorption spectra from their geometries.

The experimental investigations of oligomer conformations and their effect on electronic properties have been hampered by the multitude of conformers normally present. Some progress has been made using model compounds with a linear silicon

10.1021/jp982920y CCC: $18.00
Published on Web 01/26/1999

backbone constrained to a single conformation or to several very similar conformations.[24−26] Actual investigations of free-chain conformer mixtures seem to have been performed only on four-silicon chains[11,12,27] with hydrogen or methyl substituents.

The present paper represents the computational part of a combined theoretical and experimental investigation of a permethylated five-silicon chain, *n*-Si_5Me_{12}. We compare the geometry optimization results obtained with the MM+, MM2, MM3, and ab initio Hartree−Fock (HF) procedures. The MM procedures are commonly used for conformational analysis, and the HF method is considered quite successful in reproducing conformational energies and barriers.[28]

The number of distinct conformers of *n*-Si_5Me_{12} would be unpleasantly high even if the anti and gauche conformations were the only ones that an SiSi bond can adopt, as is the case in *n*-Si_4H_{10}.[11] This now appears extremely unlikely in the case of permethylated oligosilanes, on the basis of a recent general analysis[29,30] of a body of increasingly more accurate computational results for persubstituted linear chains that have accumulated over the years.[12,15,16,22,31−34] According to this analysis, in persubstituted chains with substituents of intermediate reduced effective size (substituent van der Waals radius and substituent-to-backbone bond length in units of backbone bond length[29]) of 0.8−1.0, steric interactions between substituents in positions 1 and 4 cause a splitting of the gauche minimum into two, named gauche ($g_\pm$, backbone dihedral angle $\omega \simeq \pm 55°$) and ortho ($o_\pm$, $\omega \simeq \pm 90°$). This splitting is analogous to the splitting of the anti minimum into two minima related by mirror-image symmetry ($a_\pm$, $\omega \simeq \pm 165°$), well recognized to take place with substituents larger than hydrogen, as a result of steric interactions of substituents in positions 1 and 3. This has recently found experimental confirmation in the case of *n*-C_4F_{10}[34] and is in agreement with the structures of certain permethylated oligosilane dendrimers.[35] As a result, *n*-Si_4Me_{10} is believed[12,22] to have three instead of two pairs of stable enantiomeric conformers, $g_\pm$, $o_\pm$, and $a_\pm$, and *n*-Si_5Me_{12} can be expected to have a correspondingly larger number of stable conformers as well. If all possible combinations of the three dihedral angle values for each bond corresponded to potential energy minima, there would be nine enantiomeric pairs of conformers plus three achiral meso conformers, for a total of 12 geometries to be optimized.

Previous computational efforts to optimize the geometries of the conformers of *n*-Si_5Me_{12} yielded the a_+a_+, a_+g_+ and g_+o_- conformers at the MNDO/2 level of calculation,[15] and the a_+a_+, a_+g_+, g_+o_-, and g_+g_+ conformers at the MM2 level.[16] We now identify two more conformers at the MM2 level, a_+o_- and o_+o_+, and additional three at the MM3 level, g_+o_+, a_+g_- and a_+o_+. Three conformers were found previously at the ab initio HF level,[21] and we now recognize them as a_+a_+, a_+o_- and o_+o_+. At this level, we identify five more, and end up with eight of the nine enantiomeric conformer pairs obtained by the MM3 method (a_+o_+ is the missing conformer). The three meso geometries do not correspond to local minima on the potential energy surfaces obtained by any of the methods of calculation.

Computational Methods

Quantum mechanical calculations were done on an IBM RS6000-590 workstation using the Gaussian 92[36a] and Gaussian 94[36b] programs with 3-21G*[37] and 6-31G*[38] basis sets. Vibrational frequencies and IR and Raman intensities were calculated in the double-harmonic approximation at the HF/3-21G* level using the Gaussian program. Molecular mechanics calculations using the MM+[39] method, as implemented in the HyperChem[40] program package, were done on an IBM compatible personal computer. Molecular mechanics calculations using the MM2[39] and MM3[41] force fields were done on a Silicon Graphics Indigo2 workstation using the Spartan[42] program and on an IBM RS6000 workstation using Allinger's[43] MM2(92)[44] and MM3(96)[45] programs. The MM+ and MM2 results are very similar, since they are based on different implementations of the same MM2[39] force field. Their differences provide an indication of the precision of such calculations.

The potential energy was calculated as a function of backbone dihedral angles, ω_i, by freezing these angles at different values while optimizing all other coordinates. The potential pitfalls involved in this approach were discussed in more detail on the simpler case of Si_4Me_{10} in ref 12. We recognize that additional conformational freedom due to possible rotations of methyl groups may increase the total number of conformers, and as a result, each of the backbone conformers that are the focus of attention here may actually correspond to a family of conformers. We have never chanced upon such additional conformational isomerism in our computational searches.

The starting points for the *n*-Si_4Me_{10} optimizations were the previously reported[12] MP2/6-31G* optimized geometries. The *n*-Si_5Me_{12} conformers were optimized starting with geometries for the conformers anticipated from combinations of backbone dihedral angles found for *n*-Si_4Me_{10}. The stationary points found upon unconstrained HF/3-21G* optimization were analyzed by calculating the second derivatives of the potential energy. Single-point energy calculations at the HF/3-21G* optimized geometries of *n*-Si_5Me_{12} were performed at the HF/6-31G* and MP2/6-31G* levels. Zero-point vibrational energy corrections calculated at the HF/3-21G* level were included in the relative energies of the potential energy minima of the conformers of *n*-Si_4Me_{10} and *n*-Si_5Me_{12}, but they had negligible influence on the relative potential energies of the conformers (∼0.1 kcal/mol). In the calculation of relative free energies, rotational entropies made even less difference, but vibrational entropies of the conformers differed significantly and caused free energy differences among conformers to differ by as much as 0.5−0.8 kcal/mol from potential energy differences. This is presumably due to significant differences in the frequencies of very low frequency vibrations (Supporting Information). It is not clear how good the harmonic approximation is in a case such as this, but free rather than potential energy differences were used in the calculation of conformer populations from Boltzmann distribution. All calculated vibrational frequencies, vibrational entropies, and the zero-point energies were scaled by 0.91 as recommended for the HF/3-21G* level of theory.[46]

The HF/3-21G* optimized *n*-Si_5Me_{12} geometries were used as starting points for unconstrained optimization by the MM+, MM2, and MM3 methods. Two-dimensional contour maps were constructed using MM energies calculated at a regular grid of 19×37 points (every 10° in ω_1 and ω_2), calculated by freezing the two backbone dihedral angles and optimizing all other coordinates. In addition, an HF/3-21G* contour map was obtained in the $150° \leq \omega_1, \omega_2 \leq 210°$ region by optimizing the geometry at 17 points with fixed values of ω_1 and ω_2.

Results and Discussion

MM2 and MM+. Since the MM+ and MM2 methods use the same force field and differ only in implementation, it is understandable that the MM+ results are very close to MM2 results and need not be considered separately. Nevertheless, in some cases the difference between the two is distressingly large (e.g., the two top curves in Figure 1 do not run parallel in the

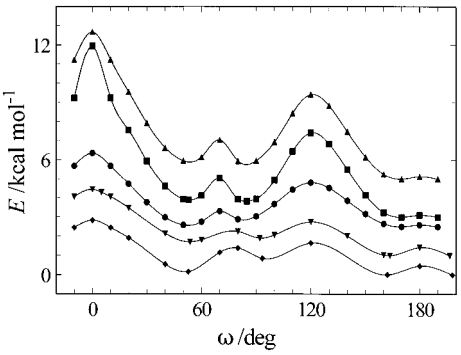

Figure 1. Ground-state potential energy curve for *n*-Si_4Me_{10} calculated as a function of backbone dihedral angle ω, with all other geometrical variables optimized (see text). Top to bottom (vertical shift up, in kcal mol^{-1}): MM2 (5), MM+ (3), MM3 (2.5), HF/3-21G* (1), MP2(FC)/3-21G*.

region of small dihedral angles). Still, the differences in the results are surely smaller than the likely deviations of either method from accurate energies, and the two programs can probably be used interchangeably. This leaves us with a comparison of the MM2, MM3, HF/3-21G*, and, at single points only, HF/6-31G* and MP2/6-31G* methods.

Conformations of *n*-Si_4Me_{10} and a Comparison of Computational Methods. It seems best to start the comparison with the previously studied *n*-Si_4Me_{10} chain, for which some experimental data on conformer energies are available. Temperature dependence of vibrational spectra measured in solution showed[27] that the a conformer is more stable than the g conformer by about 0.5 kcal mol^{-1} (the o conformer is expected to have nearly identical vibrational spectra as the g conformer and was not detected). The more recent rare-gas matrix work[12] is in qualitative agreement in that at 65 K the twisted conformers convert completely to the a form. In contrast, in the gas phase the energies of the a and g conformers must be nearly identical, since all our attempts to change their relative amounts in experiments in which they were trapped in a low-temperature matrix from vapor phase at a wide range of vapor temperatures failed and were therefore not reported in our papers on its matrix-isolated conformers.[12,19] The same techniques very easily detected the 0.9 kcal mol^{-1} difference of the gas-phase conformer energies of the closely related perfluoro-*n*-butane.[34]

Figure 1 compares the potential energy of *n*-Si_4Me_{10} as a function of the SiSiSiSi backbone dihedral angle, $0° < \omega < 180°$, as calculated now by the molecular mechanics methods MM+, MM2 and MM3, and as calculated previously[12,22] by the ab initio HF/3-21G* and MP2(FC)/3-21G* methods. Addition of corrections for the zero-point vibrational energy makes a negligible difference. All five curves agree qualitatively and contain the three minima previously predicted[12,22] for this range of ω values, at $+53°$ (g_+), $+91°$ (o_+), and $+162°$ (a_+). The ab initio results[12] for the relative energies of the o and g conformers, respectively, with respect to the a conformer, are 0.89 and 0.70 kcal mol^{-1} (HF/3-21G*), 0.79 and 0.11 kcal mol^{-1} (MP2/3-21G*), 0.65 and 0.09 kcal mol^{-1} (MP2/6-31G*), and 0.50 and 0.17 kcal mol^{-1} (MP2/6-311G**//MP2/6-31G*). The corresponding molecular mechanics energies are 0.82 and 0.89 kcal mol^{-1} (MM+), 0.81 and 0.88 kcal mol^{-1} (MM2), and 0.35 and 0.03 kcal mol^{-1} (MM3), respectively.

With regard to *n*-Si_4Me_{10} conformer energies, MM2 (and MM+) is thus similar to HF (with a conformer significantly stabilized relative to g and o conformers) and in qualitative agreement with the solution data, while MM3 resembles MP2 (with comparable energies for a and g conformers and a somewhat higher energy for the o conformer) and is in qualitative agreement with gas-phase data. The MM2 method reverses the order of energies of the o and g conformers relative to the ab initio methods, whereas the MM3 method does not. The MM2 and HF optimized geometries are also very close, with the former giving somewhat shorter SiSi bond lengths and smaller SiSiSi valence angles. The MM3 SiSi bonds lengths generally tend to be smaller and valence angles significantly larger. Since MM2 is known to make atoms appear too small and hard, and MM3 was explicitly designed to make them appear larger and softer,[47] it is understandable that MM2 exaggerates barrier heights and that the difference between MM3 and MM2 is similar to that between MP2 and HF.

The difference between HF and MP2 results is believed to result in large part from the presence of van der Waals attraction contributions in the latter, stabilizing the more compact conformers. The better agreement of the MP2 results with experimental evidence for isolated gas-phase molecules is thus no surprise. The apparent superiority of the HF results for comparison with experimental data obtained in solution must be due to a cancellation of errors and is easy to rationalize. Since the HF method ignores both the intermolecular and the intramolecular van der Waals stabilization of the alkyl groups, its results for relative energies of conformers that differ in compactness are more likely to be balanced than those of isolated-molecule MP2 calculations, which treat intramolecular but not intermolecular stabilization by van der Waals interactions. It thus appears likely that the MP2 (and MM3) results provide the best guide for estimating relative conformer energies in the gas phase, whereas the HF (and MM2 or MM+) results should be used to estimate them in solution.

No experimental data are available for the barriers between the minima. The most striking computed difference is between the high values provided by the MM2 method and the much lower values provided by MM3. It appears very unlikely that the MM2 method is correct, particularly since HF and MP2 agree well with each other and yield even lower barriers than MM3. Both MM methods underestimate the barrier between the a_+ and a_- conformers of *n*-Si_4Me_{10} calculated by the two presumably more reliable ab initio procedures.

Conformations of *n*-Si_5Me_{12}. Only qualitative experimental information is available for *n*-Si_5Me_{12}. At temperatures below ~120 K the all-anti conformer is the only detectable form of *n*-Si_5Me_{12} present in a hydrocarbon solution,[48] and it seems clear that under these conditions it is the most stable of all conformers, as it was in *n*-Si_4Me_{10}. Inspection of the results in Table 1 shows that the pattern of relative differences between the computational methods established for *n*-Si_4Me_{10} carries over, in that the more compact twisted g and o conformers are energetically unfavorable relative to the a conformer in the HF and MM2 approximations, in qualitative agreement with solution results, while in the MM3 and MP2 approximations only the o bond conformation is unfavorable and the g conformer is comparable to the a conformer. It is likely that the same rationalization of the differences applies and that the HF (MM2) results should be used in the interpretation of solution data and the MP2 results in the interpretation of gas-phase data.

The six optimized values of equilibrium SiSiSiSi dihedral angles that characterize the central SiSi bond conformations in the four-silicon chain, $g_\pm$, $o_\pm$, and $a_\pm$, provide 36 possible conformational combinations of the two backbone dihedral angles in *n*-Si_5Me_{12}, ω_1 and ω_2. The two SiSi bonds are equivalent, and only three meso geometries and nine enantiomeric pairs of geometries are unique. The meso geometries correspond to six structures, since one or the other bond can be

TABLE 1: Calculated HF and MP2 Energies (kcal mol^{-1}), Geometries, and Populations of *n*-Si_4Me_{10} and *n*-Si_5Me_{12} Conformers[a]

	ω_1[b]	ω_2[b]	HF/3-21G*					HF/6-31G*					MP2/6-31G*					
conf	deg	deg	E_{rel}	F_{rel}^{298}	P_{100}	P_{298}	P_{500}	E_{rel}	F_{rel}^{298}	P_{100}	P_{298}	P_{500}	E_{rel}	F_{rel}^{298}	P_{100}	P_{298}	P_{500}	comments
a_+	164		0.00	0.00	99	81	69	0.00	0.00	97	75	65	0.00	0.00	86	66	59	loc min
o_+	92		0.97	1.25	0	10	16	0.70	0.97	2	15	20	0.65	0.93	2	14	19	loc min
g_+	54		0.79	1.26	0	10	14	0.73	1.20	1	10	14	0.24	0.71	12	20	21	loc min
a_+a_+	164	164	0.00	0.00	99	85	70	0.00	0.00	99	80	64	0.00	0.00	94	70	56	loc min
a_+a_-	171	−170	0.69					0.74					0.89					saddle
a_+g_+	162	55	0.81	1.26	0	5	7	0.82	1.27	0	5	7	0.29	0.74	5	10	10	loc min
a_+g_-	169	−70	1.64	1.44	0	4	9	1.39	1.19	0	5	11	1.23	1.02	0	6	12	loc min
a_+o_+	165[c]	92[c]	1.48					1.48					1.46					no min
a_+o_-	167	−91	1.07	1.37	0	4	7	0.82	1.12	0	6	8	0.75	1.05	1	6	8	loc min
g_+g_+	57	53	2.07	2.75	0	1	3	1.74	2.42	0	1	4	0.88	1.56	0	5	7	loc min
g_+o_+	68	93	2.67	3.09	0	0	1	2.04	2.46	0	1	2	1.79	2.21	0	1	2	loc min
g_+o_-	66	−104	2.64	3.08	0	0	1	2.16	2.60	0	0	2	1.60	2.04	0	1	3	loc min
o_+o_+	89	89	2.18	2.83	0	0	1	1.63	2.28	0	1	2	1.49	2.13	0	1	2	loc min
o_+o_-	76	−74	3.72					3.48					2.69					saddle

[a] Total HF/3-21G* energy (au): $a_\pm$-*n*-Si_4Me_{10}, −1544.088 312; $a_\pm a_\pm$-*n*-Si_5Me_{12}, −1910.406 853. Relative potential energies (E_{rel}) include scaled (0.91) HF/3-21G* zero-point vibrational energies. HF/6-31G* and MP2/6-31G* energies were calculated at HF/3-21G* optimized geometries. Relative free energies (F_{rel}^{298}) at 298 K were obtained by adding rotational entropy and scaled vibrational entropy contributions and were used to compute % populations P_t at three temperatures. [b] Fully optimized HF/3-21G* geometries. [c] Constrained dihedral angles (a calculation at g_+g_- geometry with constrained dihedral angles gave very high energy).

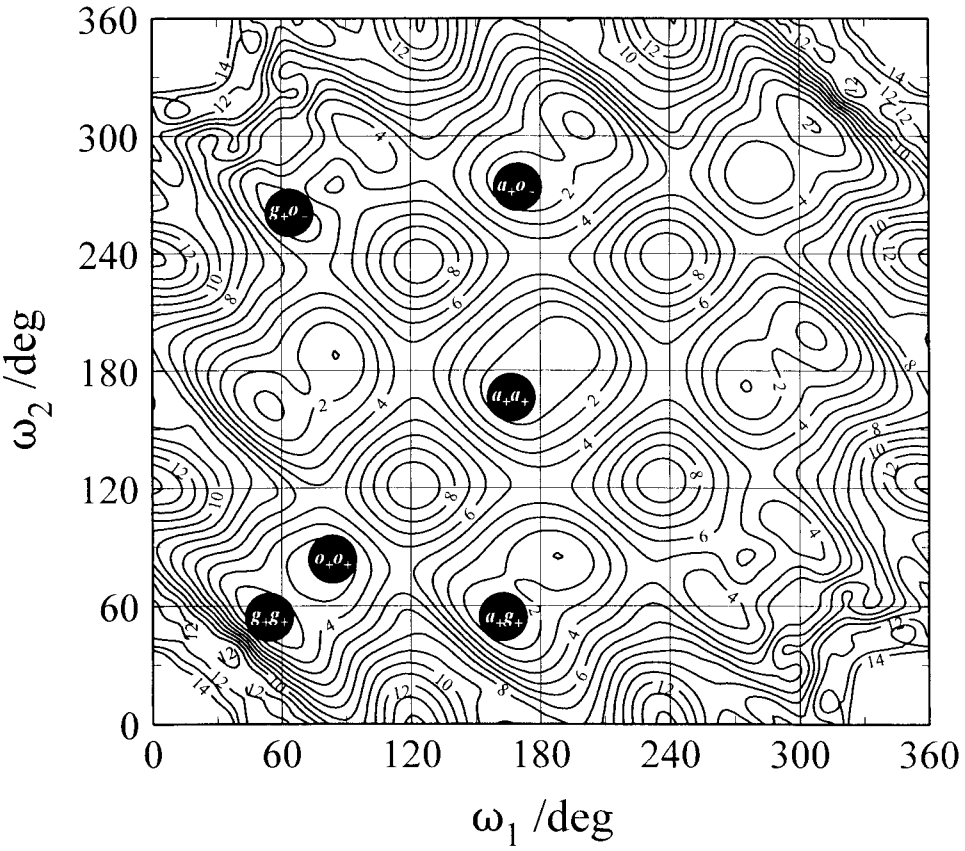

Figure 3. MM2 conformational energy contour map for *n*-Si_5Me_{12} as a function of the two backbone dihedral angles ω_1 and ω_2. Inequivalent MM2 optimized geometries of stable conformers are indicated.

twisted in the positive sense. In three of the nine enantiomeric pairs of geometries the two bonds are twisted equally, but the other 6 correspond to 12 enantiomeric pairs of minima, since each of the 2 bonds is twisted differently.

For the 12 independent geometries to optimize, we have chosen those characterized by the following pairs of the two independent SiSiSiSi dihedral angles ω_1 and ω_2: a_+a_+ (164, 164), a_+a_- (164, −164), a_+g_+ (164, 54), a_+g_- (164, −54), a_+o_+ (164, 92), a_+o_- (164, −92), g_+g_+ (54, 54), g_+g_- (54, −54), g_+o_+ (54, 92), g_+o_- (54, −92), o_+o_+ (92, 92), and o_+o_- (92, −92). It was not clear a priori how many of the 12 combinations will correspond to actual potential energy minima and whether additional minima might not be present at other values of dihedral angles. The latter issue was addressed by computing ground-state potential energy surface contour maps with ω_1 and ω_2 as the variables. Since the qualitative features of the *n*-Si_4Me_{10} potential energy curve computed with MM methods agreed well with those computed with ab initio methods, we only used the inexpensive methods, MM+ (Figure 2 in Supporting Information), MM2 (Figure 3), and MM3 (Figure 4). Since the MM+ and the MM2 results were very similar, Figure 2 was relegated to the Supporting Information.

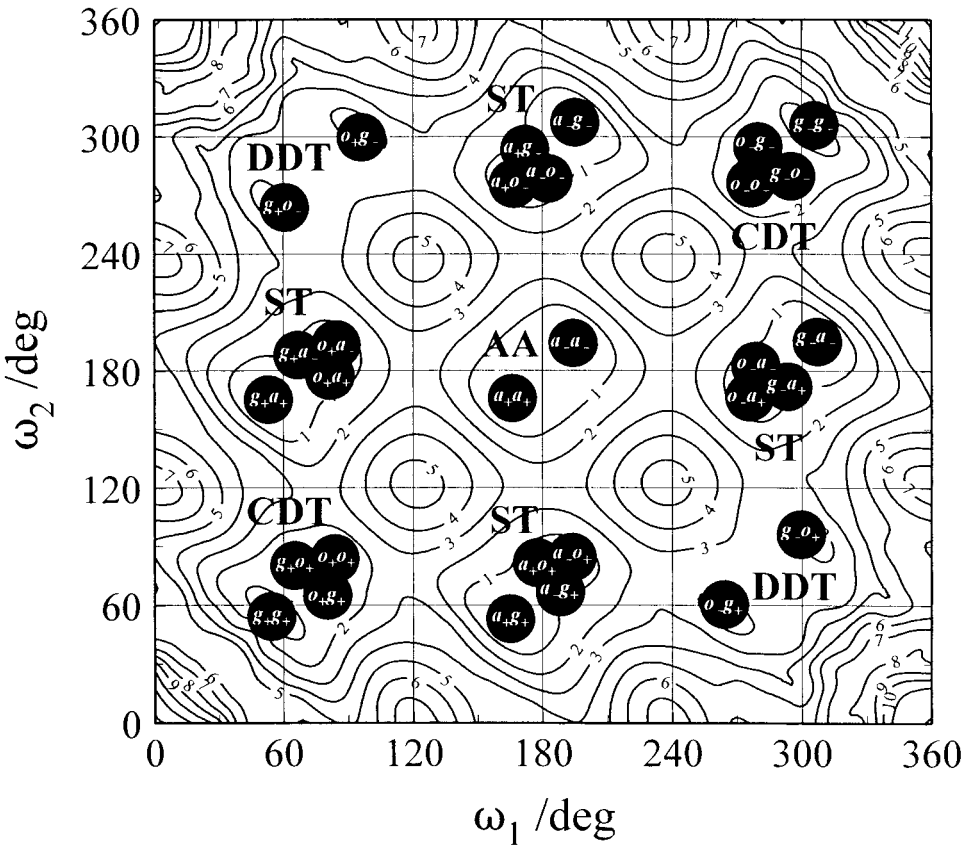

Figure 4. MM3 conformational energy contour map for *n*-Si_5Me_{12} as a function of the two backbone dihedral angles ω_1 and ω_2. All MM3 optimized geometries of stable conformers are indicated, and the nine groups of related conformers are labeled.

Owing to the equivalence of the two dihedral angles and to mirror image symmetry, the potential energy is equal at points with dihedral angles (ω_1, ω_2), (ω_2, ω_1), ($-\omega_1$, $-\omega_2$), and ($-\omega_2$, $-\omega_1$), and the contour maps contain mirror reflection symmetry lines $\omega_2 = \omega_1$ and $\omega_2 = 180° - \omega_1$. Low-energy regions were found only in the vicinity of most of the 12 conformational combinations listed above, and we felt comfortable in limiting ab initio searches for low-energy conformations to the 12 starting points defined by results for *n*-Si_4Me_{10}. Unconstrained HF/3-21G* optimization yielded eight stable conformers and one meso saddle point (a_+a_-), as judged by the computed second derivatives, while the other two meso geometries and the a_+o_+ choice did not lead to any nearby stationary points and ultimately produced one of the eight stable conformers (Table 1). A HF/3-21G* transition-state calculation yielded a second meso geometry (o_+o_-) as a saddle point connecting the o_+g_-, g_+o_- enantiomeric pair. The HF/3-21G* optimized geometries for the eight stable enantiomeric conformer pairs of *n*-Si_5Me_{12} and two meso saddle point geometries are shown in Figures 5 (one set of enantiomers only) and 6, respectively.

Unconstrained MM optimizations of the eight stable conformers were performed starting with the HF/3-21G* optimized geometries. Only six stable conformers were found by the MM+ and MM2 methods, at geometries near those found at the HF level, and no a_+g_- and g_+o_+ conformer minima were found. The MM3 optimizations found the same eight stable conformers as the HF optimizations, at similar geometries (Tables 2 and 3), and a ninth one, a_+o_+. A comparison of the MM2, MM3, and HF optimized dihedral angles is shown in Figure 7, and the great similarity of the three sets of results is apparent. The absence of a local minimum at the a_+g_- and g_+o_+ geometries in the MM2 results and the presence of a local minimum at the a_+o_+ geometry in the MM3 results are the most noticeable difference relative to the HF results. Its practical significance is uncertain, since the energies and geometries of these conformers are very close to those of the a_+o_-, o_+o_+, and a_+g_+ conformers, respectively, and the barriers separating the members of the a_+g_-, a_+o_- pair, the g_+o_+, o_+o_+ pair, and the a_+o_+, a_+g_+ pair are surely minute. The locations of the minima are indicated by black circles in the contour diagrams. In order not to block the view of the contour lines, Figures 2 and 3 show only a minimal set from which the others can be deduced by the two mirror-symmetry operations. In Figure 4 all the minima are shown in order to facilitate the discussion of conformer interconversion.

The conformer minima of *n*-Si_5Me_{12} fall into nine groups, where members of each group differ only by $a_+ \leftrightarrow a_-$, $g_+ \leftrightarrow o_+$, or $g_- \leftrightarrow o_-$ interchanges (Figure 4). Each of the first three groups contains only two enantiomers, whereas the remaining six groups occur as three pairs, with pair members related by mirror-image symmetry. The first group (AA) is formed by a pair of enantiomers of the "all-anti" type (a_+a_+, a_-a_-), while those in the second and third groups (DDT) are of the "disrotatory doubly twisted" type (g_+o_-, g_-o_+ and o_-g_+, o_+g_-). The fourth and fifth groups (ST) each consists of three "singly twisted" conformers: g_+a_+, g_+a_-, o_+a_- and a_+g_+, a_-g_+, a_-o_+. At the MM2 level g_+a_-, a_-g_+, and their enantiomers are missing (this was also the case in ab initio calculations[33] on *n*-C_5F_{12}), and at the MM3 level o_+a_+ and a_+o_+ are also present. The members of the sixth and seventh group (ST) are mirror images of the members of the fourth and fifth groups. The eighth group (CDT) has four "conrotatory doubly twisted" conformers: g_+g_+, g_+o_+, o_+g_+, o_+o_+. At the MM2 level g_+o_+, o_+g_+, and their enantiomers are missing (this was also the case in ab initio calculations[33] on *n*-C_5F_{12}). The ninth group (CDT) contains the mirror images of the members of the eighth group. The smaller

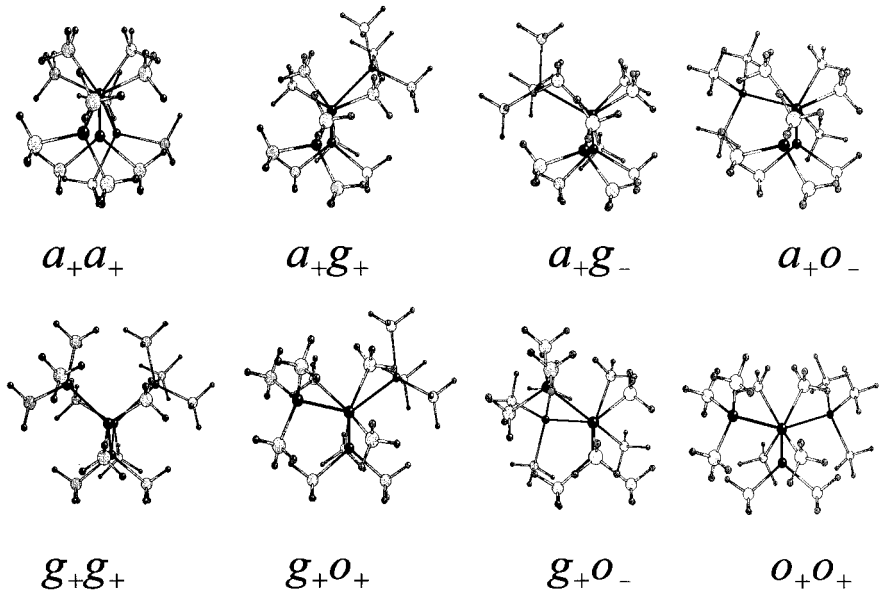

Figure 5. HF/3-21G* optimized geometries for the conformers of *n*-Si_5Me_{12}, viewed in the Si_2-Si_4 direction.

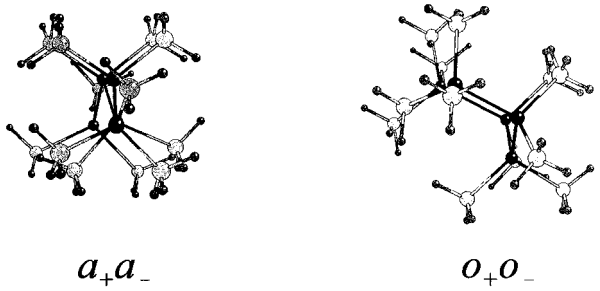

Figure 6. HF/3-21G* optimized geometries for the a_+a_- and o_+o_- transition states of *n*-Si_5Me_{12}, viewed in the Si_2-Si_4 direction.

number of disrotatory relative to conrotatory doubly twisted conformers is due to strong steric interactions in the former case (like a_+a_-, g_+g_- and o_+o_- also lie on the ridge that contains transition states for enantiomer interconversion and would not be expected to correspond to potential surface minima).

At the HF/6-31G* level of calculation, the all-anti a_+a_+ conformer is the most stable and the singly twisted conformers are about 0.8 kcal mol^{-1} less stable, except for a_+g_-. The a_+g_- conformer and the conrotatory doubly twisted conformers are about 1.5 kcal mol^{-1} less stable, while the disrotatory doubly twisted conformer is about 2 kcal mol^{-1} less stable. The differences are accentuated when free rather than potential energies are considered. The relative destabilization of the singly twisted a_+g_- conformer, the absence of the a_+o_+ conformer (except in MM3), and the absence of minima at the meso a_+a_-, o_+o_-, and g_+g_- geometries can all be understood in terms of the rules for terminal-group twisting preferences deduced previously for an A_4X_{10} chain.[29,30,32,33] Only the great similarity of the energies of the doubly twisted g_+o_+ and g_+o_- conformers runs against expectations. If our assumptions concerning the applicability of the HF results are correct, the a_+a_+ conformer will dominate in the room-temperature solution equilibrium, and significant amounts of the singly twisted a_+g_+ and a_+o_- conformers will be present. At low temperatures, the a_+a_+, a_-a_- enantiomeric pair is predicted to be practically the only conformer present, just as the a_+, a_- pair is in the case of *n*-Si_4Me_{10},[12] and this agrees with the observations mentioned above.

At the MP2/6-31G* level of calculation, the a_+a_+ conformer is still predicted to be the most stable, but the singly twisted a_+g_+ conformer now is of comparable potential energy, although its free energy is significantly higher. The potential energy of the singly twisted a_+o_- and the doubly twisted g_+g_+ is about 0.8 kcal mol^{-1} higher, a_+g_- is again destabilized further, and the remaining doubly twisted conformers are even less stable, although less so than at the HF/6-31G* level. At room-temperature gas-phase equilibrium, one would anticipate the a_+a_+ conformer to dominate and a_+g_+ to be present in significant amounts, followed by the a_+o_-, a_+g_-, and g_+g_+ conformers.

The conformer interconversion pathways are similar in the contour diagrams in Figures 2−4 and would presumably also remain similar in those obtained at the HF and MP2 levels, which were prohibitively expensive to obtain. Conformer interconversions are facile within each of the nine groups identified above. We have identified two pairs of equivalent transition states as judged by the HF/3-21G* frequency calculation, located at the meso a_+a_-, a_-a_+ and o_+o_-, o_-o_+ pairs of geometries (Figure 6).

The first of these saddle point pairs connects the two members of the AA (first) group (Figure 4), the a_+a_+ and a_-a_- enantiomers (Figure 5), with an activation energy of 0.7 kcal mol^{-1}. These enantiomers can interconvert in two possible equivalent ways, since one or the other internal SiSi bond can twist first. The a_+a_- and a_-a_+ geometries are favored over a symmetric transition state with both dihedral angles equal to 180° (Figure 8). The same conclusion is reached from the MM+, MM2, and MM3 contour maps in Figures 2 (Supporting Information), 3, and 4.

The second pair of equivalent saddle points connects conformers within the DDT (second and third) groups (Figure 4) with an activation energy of 3.7 kcal mol^{-1}. The g_+o_- and o_+g_- conformers (Figure 5) interconvert via the o_+o_- transition state (Figure 6) and the g_-o_+ and o_-g_+ conformers (Figure 5) via the o_-o_+ transition state (Figure 6). The dihedral angles in these transition states are 75° and thus are severely distorted from the usual ortho values of about 90° toward the gauche values of about 55°. We have not attempted to find out whether the nominally remaining meso geometries, g_+g_- and g_-g_+, are alternative transition states for the interconversion within the two DDT groups or whether they have merged with the o_+o_-, o_-o_+ pair, but from the contour diagrams in Figures 2−4 it

TABLE 2: Selected Parameters from Optimized Geometries of the Conformers[a] of *n*-Si_4Me_{10} and *n*-Si_5Me_{12}

conf	method[b]	R_{12} Å	R_{23} Å	R_{34} Å	θ_{123} deg	θ_{234} deg	ω_{1234} deg	ω_{6123} deg	ω_{23415} deg
a_+	HF	2.356	2.359	2.356	112	112	164	168	168
	MP2	2.330	2.330	2.330	110	110	162	167	167
	MM+	2.350	2.345	2.350	111	111	169	174	174
	MM2	2.346	2.343	2.346	111	111	167	173	173
	MM3	2.335	2.340	2.335	116	116	166	171	171
o_+	HF	2.355	2.365	2.355	114	114	92	172	172
	MP2	2.330	2.335	2.330	112	112	93	−172	−172
	MM+	2.346	2.341	2.346	114	114	85	−177	−177
	MM2	2.344	2.341	2.344	113	113	86	−177	−177
	MM3	2.336	2.342	2.336	117	117	84	−174	−174
g_+	HF	2.355	2.358	2.355	116	116	54	165	165
	MP2	2.329	2.327	2.329	114	114	53	164	164
	MM+	2.340	2.340	2.340	115	115	53	166	166
	MM2	2.339	2.340	2.339	115	115	54	166	166
	MM3	2.335	2.340	2.335	117	117	52	166	166

conf	method[b]	R_{12} Å	R_{23} Å	R_{34} Å	R_{45} Å	θ_{123} deg	θ_{234} deg	θ_{345} deg	ω_{1234} deg	ω_{2345} deg	ω_{6123} deg	ω_{34516} deg
a_+a_+	HF	2.357	2.361	2.361	2.357	112	111	112	164	164	167	167
	MM+	2.349	2.349	2.349	2.349	111	110	111	167	168	173	173
	MM2	2.345	2.346	2.346	2.345	111	110	111	166	166	173	173
	MM3	2.335	2.339	2.339	2.335	116	116	116	166	166	170	170
a_+a_-	HF	2.359	2.361	2.361	2.359	112	113	112	171	−171	166	−166
a_+g_+	HF	2.357	2.359	2.360	2.355	112	115	116	162	55	167	165
	MM+	2.354	2.340	2.343	2.341	111	114	115	162	54	167	173
	MM2	2.349	2.342	2.340	2.340	111	114	115	162	54	167	172
	MM3	2.337	2.338	2.339	2.335	118	118	116	165	53	167	171
a_+g_-	HF	2.357	2.358	2.362	2.365	112	115	117	169	−70	168	−144
	MM3	2.341	2.341	2.343	2.343	116	119	119	172	−67	172	−153
a_+o_+	MM3	2.343	2.342	2.338	2.336	117	118	118	178	82	174	−174
a_+o_-	HF	2.357	2.360	2.366	2.356	112	113	114	167	−91	167	171
	MM+	2.350	2.345	2.345	2.345	111	113	114	171	−86	175	178
	MM2	2.347	2.344	2.344	2.344	111	113	114	169	−86	173	177
	MM3	2.336	2.339	2.339	2.336	116	117	117	166	−84	171	173
g_+g_+	HF	2.358	2.358	2.358	2.358	116	119	116	57	57	159	159
	MM+	2.340	2.334	2.334	2.340	115	119	115	54	54	165	165
	MM2	2.339	2.336	2.336	2.339	115	119	115	54	54	165	165
	MM3	2.336	2.336	2.336	2.339	118	120	118	54	54	164	165
g_+o_+	HF	2.366	2.361	2.366	2.355	117	116	114	68	93	143	−173
	MM3	2.336	2.340	2.341	2.340	119	120	118	65	80	157	−175
g_+o_-	HF	2.354	2.361	2.371	2.357	118	117	115	66	−104	171	176
	MM+	2.338	2.340	2.338	2.345	116	117	115	64	−99	172	−178
	MM2	2.337	2.341	2.341	2.345	116	117	115	64	−99	173	−178
	MM3	2.333	2.341	2.346	2.338	119	120	118	60	−96	173	178
o_+o_+	HF	2.357	2.366	2.366	2.357	114	116	114	89	89	−171	−171
	MM+	2.346	2.340	2.340	2.346	115	117	115	80	80	−179	−179
	MM2	2.345	2.342	2.342	2.345	113	116	113	84	84	−176	−177
	MM3	2.337	2.343	2.343	2.347	117	119	117	84	84	−173	−173
o_+o_-	HF	2.368	2.364	2.362	2.354	118	119	118	76	−74	135	−169

[a] See Figure 13 for atom numbering. [b] HF/3-21G*, MP2/3-21G*.

appears that they are at higher energies if they have separate existence all.

In each of the four symmetry-related ST groups (fourth to seventh) one conformer is a high-energy intermediate for the interconversion of the two others (in the MM3 contour map, two conformers are such intermediates). Thus, g_+a_- (in MM3, also a_+o_+) is an intermediate in the interconversion of g_+a_+ and o_+a_- (at the MM2 level this geometry does not contain an intermediate but is close to a transition state). Finally, in each of the CDT groups (eighth and ninth), two of the conformers serve as symmetry-related high-energy intermediates for the interconversion of the other two. Thus, g_+o_+, and o_+g_+ serve as intermediates in the interconversion of g_+g_+ and o_+o_+ (at the MM2 level these geometries do not contain intermediates but are close to transition states).

More significant barriers separate these nine distinct groups of conformers. Not surprisingly, the conversion of a doubly twisted conformer into an all-anti conformer proceeds by a stepwise rotation of first one and then the other dihedral angle. However, the motions involved are intricate. For instance, the path from o_+o_+ to a_+a_+, which nominally requires an increase of both ω_1 and ω_2 from about 90° to about 165°, takes the molecule first to a_+g_+, then a_-g_+, and then a_-o_+ before the goal is reached, in the process changing both dihedral angles in the "wrong" direction at one or another time.

All-Anti Conformer of *n*-Si_5Me_{12}. All three ab initio and two of the MM methods of calculation agree that the a_+a_+, a_-a_- enantiomer pair is the global minimum, and only the MM3 calculation places this conformer 0.04 kcal mol^{-1} above the a_+g_+ minimum. The increased valence angles (Table 2) are in accord with the argument that this splitting of the classical a,a minimum into two enantiomeric minima is caused by 1,3 repulsions. At the HF/3-21G* level of theory, the a_+a_+

TABLE 3: Calculated HF, MP2, MM+, MM2, and MM3 Energies and Geometries of *n*-Si_4Me_{10} and *n*-Si_5Me_{12} Conformers

	HF/3-21G*[a]			HF/6-31G*[b]	MP2/6-31G*[b]	MM+			MM2			MM3		
conformer	E_{rel}	ω_1	ω_2	E_{rel}	E_{rel}	E_{rel}	ω_1	ω_2	E_{rel}	ω_1	ω_2	E_{rel}	ω_1	ω_2
a_+	0.00	164		0.00	0.00	0.00	169		0.00	167		0.00	166	
o_+	0.97	92		0.70	0.65	0.82	85		0.81	86		0.35	84	
g_+	0.79	54		0.73	0.24	0.89	53		0.88	54		0.03	52	
a_+a_+	0.00	164	164	0.00	0.00	0.00	167	168	0.00	166	166	0.04	166	166
a_+g_+	0.81	162	55	0.82	0.29	0.63	162	54	0.63	162	54	0.00	165	53
a_+g_-	1.6	169	−70	1.4	1.2							1.01	172	−67
a_+o_+	1.5			1.5	1.5							0.67	178	82
a_+o_-	1.1	167	−91	0.82	0.75	0.85	171	−86	0.86	169	−86	0.43	166	−84
g_+g_+	2.1	57	53	1.7	0.88	1.72	54	54	1.73	54	54	0.23	54	54
g_+o_+	2.7	68	93	2.0	1.8							1.28	65	80
g_+o_-	2.6	66	−104	2.2	1.6	2.98	64	−99	2.98	64	−99	1.24	60	−96
o_+o_+	2.2	89	89	1.6	1.5	2.10	80	80	2.11	84	84	0.97	84	84

[a] Fully optimized HF/3-21G* geometries (ω in deg); zero-point vibrational energy corrections scaled by 0.91. [b] Energies in kcal mol^{-1} calculated at HF/3-21G* optimized geometries, with scaled HF/3-21G* zero-point vibrational energies.

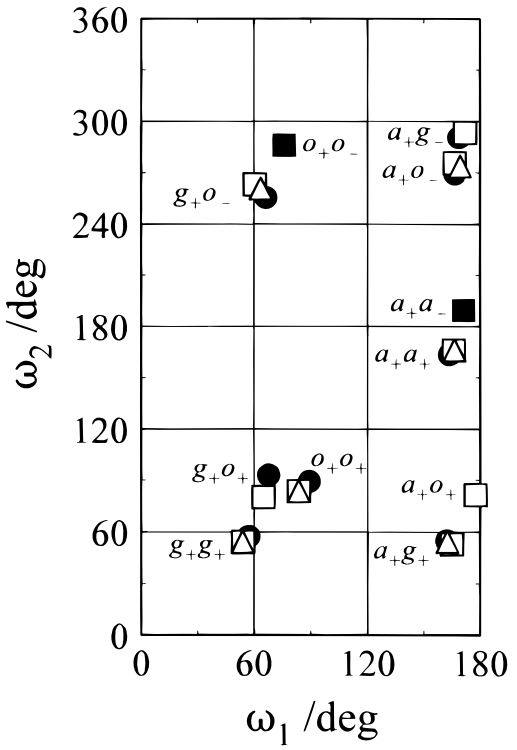

Figure 7. Optimized dihedral angles ω_1 and ω_2 in the conformers of *n*-Si_5Me_{12}: HF/3-21G*, ● (transition states, ■); MM3, □; MM2, △.

conformer has optimized dihedral angles of 163.6° and 163.5°, identical within the accuracy of the convergence.

Singly Twisted Conformers of *n*-Si_5Me_{12}. The above-noted simple considerations[29,30,32,33] of the preferred sense of end-group twisting in a persubstituted four-membered chain suggest that the a_+g_+ and a_+o_- conformations should be favored over a_+g_- and a_+o_+, and this is observed. The a_+g_- geometry exhibits increased steric interactions between the methyl substituent in position 2 of the backbone and the backbone atom Si(5) and two of its methyl substituents (Figure 5). In the a_+o_- geometry the terminal Si(5) trimethylsilyl group has rotated to relieve these 1,4 substituent−substituent and 1,4 substituent−backbone interactions. Considerable deviations of the optimized dihedral angles from the values anticipated for the a_+g_- conformer result.

To incorporate the o_+ orientation in the a_+o_+ conformer, the trimethylsilyl group on the opposite end is pushed back into the central silicon backbone plane. This results in increased 1,3-substituent interactions between substituents on the 1,3 and 2,4 positions of the backbone and is partially compensated by increased SiSiSi valence angles (Table 2).

Doubly Twisted Conformers of *n*-Si_5Me_{12}. Consideration[29,30,32,33] of end-group twisting preferences in a persubstituted four-membered chain suggests that the g_+g_+, g_+o_-, and o_+o_+ conformations are favored over g_+g_-, g_+o_+, and o_+o_-, respectively. This expectation is fulfilled except for the relatively favorable HF energy of g_+o_+, which however has strongly distorted dihedral angles of 66.3° and −104.5°. The MP2 energies are in the anticipated order, but their difference is small. In the g_+o_- geometry, both end groups are on the same side of the central SiSiSi plane and therefore more torsional relaxation is possible. Even though the terminal trimethylsilyl groups are on opposite sides of the central SiSiSi plane in the g_+o_+ conformation, there is little room for torsional relaxation of the o orientation because of increased 1,4-substituent interaction that would result from an increase of the torsional angle.

HF/3-21G* and single-point HF/6-31G* calculations yield similar results except that the latter places the o_+o_+ conformer 0.1 kcal mol^{-1} below g_+g_+. Five-membered chains might perhaps provide a favorable opportunity for an observation of an o conformer, containing the ordinarily least stable of the dihedral angles.

Conformational Energy Increments. From the HF, MP2, MM2, and MM3 conformation energies calculated for *n*-Si_4Me_{10} and *n*-Si_5Me_{12}, additive sets of three intrinsic bond-conformation energies E_α and 12 two-bond interaction energies $E_{\alpha\beta}$ were derived in the hope that they will permit a prediction of the relative energies E of chain conformations for chain lengths greater than $n = 5$ from the additive expression

$$E = E(a_+a_+a_+...) + \sum_\alpha n_\alpha E_\alpha + \sum_{\alpha\beta} n_{\alpha\beta} E_{\alpha\beta} \qquad (\alpha,\beta = a_\pm, o_\pm, g_\pm) \quad (1)$$

where the first sum is over all SiSiSiSi dihedral angles in the backbone and the second sum is over all pairs of adjacent dihedral angles in the backbone. The bond-conformation energy constants E_α are taken from the results of calculations for *n*-Si_4Me_{10} and are defined as the intrinsic conformation energy in the absence of any interactions with neighboring bonds, relative to the energy of the conformers a_+ and a_- ($E_a = 0$). The two-bond interaction energy increments $E_{\alpha\beta}$ are assigned values required for eq 1 to reproduce the relative energies calculated for the conformations of *n*-Si_5Me_{12}. The increments $E_{\alpha\beta}$ represent the extra amounts by which the 12 possible distinct adjacent dihedral angle combinations differ from those predicted by adding the bond-conformation energies E_α alone.

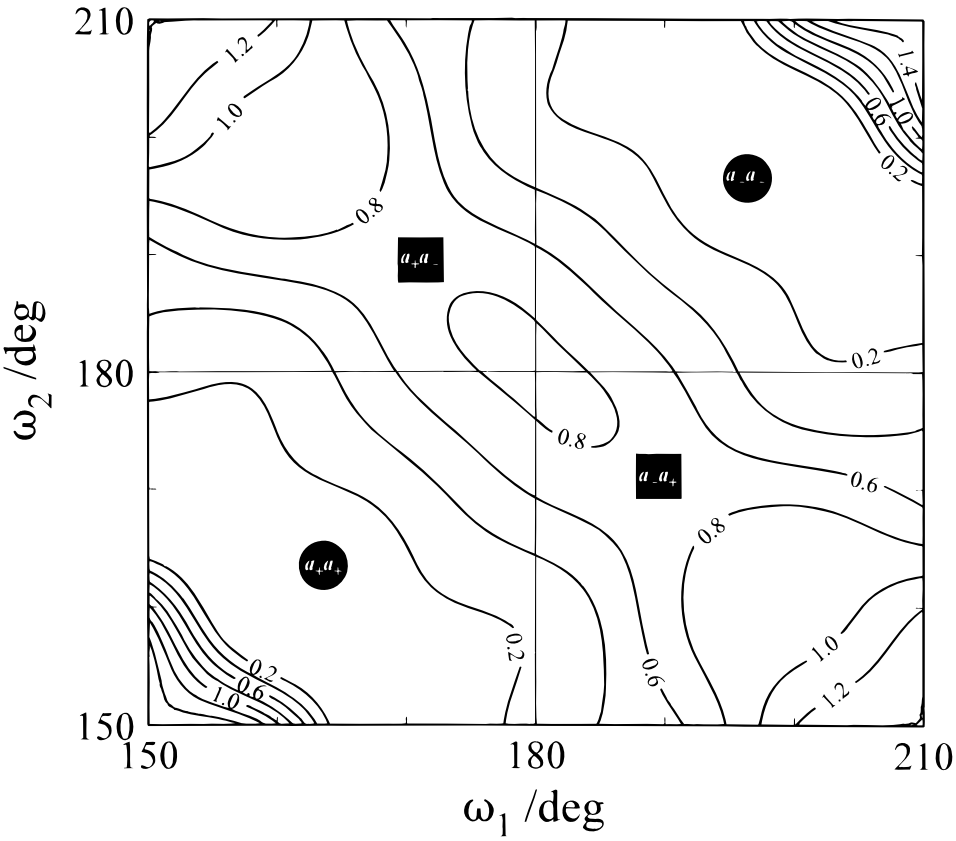

Figure 8. HF/3-21G* conformational energy contour map for *n*-Si_5Me_{12} as a function of the two backbone dihedral angles ω_1 and ω_2. HF/3-21G* optimized geometries of the a_+a_+ and a_-a_- conformers and the a_+a_- and a_-a_+ saddle points are indicated.

The intrinsic bond-conformation energies E_α and the interaction increments $E_{\alpha\beta}$ are collected in Table 4 for all four methods of calculation. Before recommending their use in deriving conformation energies in longer chains, we need to test them. So far, this has been done for several conformations calculated at the MM3 level for *n*-Si_6Me_{14} (Table 5), and the comparisons between the predicted and calculated conformer energies are quite good. The largest differences are seen for adjacent bond conformations for which there is no local minimum or where a restricted dihedral energy was used in the calculation of the interaction constant (as in the $a_-a_-a_+$ conformer where the a_-a_+ conformation is not a minimum at the MM3 level). We intend to perform more exhaustive tests in the future.

Calculated IR and Raman Spectra for the Conformers of *n*-Si_5Me_{12}. The vibrational frequencies and IR as well as Raman intensities calculated for the eight stable conformers at the HF/3-21G* level are compiled in Table 6 (Supporting Information), and the full spectra are shown in Figures 9 and 10 (Supporting Information). There are 153 normal modes for each conformer, making the calculated IR and Raman spectra very crowded.

Below 300 cm^{-1} one finds the SiSiSi, SiSiC and CSiC deformations, and methyl, trimethylsilyl, and dihedral torsion normal modes. The frequency variation of these normal modes among the conformers ranges from 1 to 15 cm^{-1}. The calculated IR and Raman intensities are extremely weak, with the exception of three normal modes centered around 200 cm^{-1}, one centered around 220 cm^{-1} and three centered around 250 cm^{-1}, which are still very weak, with an average calculated IR intensity of ~9 km mol^{-1} and calculated Raman scattering cross-sections 2 orders of magnitude smaller than the most intense Raman line.

The 300−500 cm^{-1} region appears more promising for analytical purposes. There are four distinct Si−Si stretching modes that involve very little substituent motion. For any one conformer, their frequencies are separated by more than 20 cm^{-1} (Table 7). Two lower frequency modes (centered around 340 and 380 cm^{-1}) belong to the symmetric and the antisymmetric stretching of the terminal Si−Si bonds, respectively, and two higher frequency modes (centered around 430 and 475 cm^{-1}) belong to the symmetric and the antisymmetric stretching of the internal Si−Si bonds, respectively. The variation of the frequencies of these modes among the conformers seems to be correlated with changes in the SiSiSi valence angles in that the separation between the symmetric and the antisymmetric stretching frequencies increases as the valence angles increase (Table 2). The IR intensities for these four vibrational modes are calculated to be 2−3 orders of magnitude weaker than typical intensities in the mid-IR region, and they will be difficult to observe. However, in the Raman spectrum at least two of these modes are calculated to be fairly intense relative to the most intense Raman line. Of these four vibrational transitions, the symmetric stretching of the terminal bonds at ~340 cm^{-1} shows the largest variation of individual vibrational frequencies among the eight conformers, up to 20 cm^{-1}. With an increasing twist in one and, even more so, two different dihedral angles, this vibrational frequency decreases. This region offers the best opportunity for obtaining information on individual conformers in a low-temperature mixture and is shown enlarged in Figure 11.

The 600−900 and 1200−1400 cm^{-1} regions are dominated by SiCH deformation and SiC stretching and by CH_3 deformation vibrations, respectively. The most intense of these vibrational transitions is centered around 815 cm^{-1} (Figure 12) and

TABLE 4: Additive Conformational Energy Increment Scheme for *n*-Si_nMe_{2n+2} Chains[a]

	bond-interaction energies $E_{\alpha\beta}$						bond-conf
$\alpha\backslash\beta$	a_+	o_+	g_+	a_-	o_-	g_-	energies E_α
				HF/3-21G*			
a_+	0.00	0.51	0.02	0.69	0.13	0.81	$a_\pm$, 0.00
o_+	0.51	0.26	0.94	0.13	1.76	0.84	$o_\pm$, 0.97
g_+	0.02	0.94	0.52	0.81	0.84		$g_\pm$, 0.79
a_-	0.69	0.13	0.81	0.00	0.51	0.02	
o_-	0.13	1.76	0.84	0.51	0.26	0.94	
g_-	0.81	0.84		0.02	0.94	0.52	
				HF/6-31G*			
a_+	0.00	0.76	0.09	0.74	0.12	0.67	$a_\pm$, 0.00
o_+	0.76	0.20	0.57	0.12	2.10	0.77	$o_\pm$, 0.70
g_+	0.09	0.57	0.24	0.67	0.77	-	$g_\pm$, 0.73
a_-	0.74	0.12	0.67	0.00	0.76	0.09	
o_-	0.12	2.10	0.77	0.76	0.20	0.57	
g_-	0.67	0.77		0.09	0.57	0.24	
				MP2/6-31G*			
a_+	0.00	0.87	0.05	0.89	0.10	0.96	$a_\pm$, 0.00
o_+	0.87	0.20	0.91	0.10	1.40	0.71	$o_\pm$, 0.65
g_+	0.05	0.91	0.40	0.96	0.71		$g_\pm$, 0.24
a_-	0.89	0.10	0.96	0.00	0.87	0.05	
o_-	0.10	1.40	0.71	0.87	0.20	0.91	
g_-	0.96	0.71	-	0.05	0.91	0.40	
				MM2[b]			
a_+	0.00	1.31	−0.25	1.44	0.04	2.93	$a_\pm$, 0.00
o_+	1.31	0.48	2.37	0.04	4.04	1.29	$o_\pm$, 0.81
g_+	−0.25	2.37	−0.04	2.93	1.29	6.26	$g_\pm$, 0.88
a_-	1.44	0.04	2.93	0.00	1.31	−0.25	
o_-	0.04	4.04	1.29	1.31	0.48	2.37	
g_-	2.93	1.29	6.26	−0.25	2.37	−0.04	
				MM3			
a_+	0.00	0.32	−0.03	1.02	0.08	0.98	$a_\pm$, 0.00
o_+	0.32	0.27	0.87	0.08	2.99	0.86	$o_\pm$, 0.35
g_+	−0.03	0.87	0.17	0.98	0.86	3.43	$g_\pm$, 0.03
a_-	1.02	0.08	0.98	0.00	0.32	−0.03	
o_-	0.08	2.99	0.86	0.32	0.27	0.87	
g_-	0.98	0.86	3.43	−0.03	0.87	0.17	

[a] In kcal mol^{-1}; HF/3-21G*, HF/6-31G*, and MP2/6-31G* energies were all obtained at HF/3-21G* optimized geometries, and MM2 and MM3 energies at MM2 and MM3 optimized geometries, respectively. For the a_+a_- geometry, which is not a local minimum, the HF/3-21G* optimized saddle point geometry was used for HF/3-21G*, HF/6-31G*, and MP2/6-31G* energies, and both backbone dihedral angles were set to 162° (the MP2/3-21G* optimized value for Si_4Me_{10}) for MM2 and MM3 energies. [b] MM+ values are nearly identical.

TABLE 5: MM3 Energies of Some *n*-Si_6Me_{14} Conformations from Additive Increments and from Calculation (kcal mol^{-1})

conf	E_{incr}	E_{MM3}
$a_+a_+a_+$	0.00	0.00
$a_-a_-a_+$	1.02	0.58
$o_+a_+a_+$	0.67	0.83
$g_+o_+o_+$	1.87	1.80
$g_+g_+a_+$	0.20	0.20
$a_-o_+g_+$	1.33	1.24
$a_+o_-a_+$	0.51	0.44
$a_+g_+a_+$	−0.03	−0.05
$a_-o_+a_+$	0.75	0.86

has a calculated IR intensity of 500 km mol^{-1}. This mode is at a distinctly lower frequency in the a_+a_+ conformer. Unfortunately, the vibrational frequency variation between the singly and doubly twisted conformers is less than 1 cm^{-1}, thus making it unlikely that it will be possible to gain any information on the other individual conformers. Centered around 840 cm^{-1} is a moderately intense vibrational mode for all singly and doubly twisted conformers. This vibrational mode has negligible IR intensity in the a_+a_+ conformer and is at a somewhat higher frequency in the doubly twisted than the singly twisted conformers. However, the frequency variation among conformers is only ∼2−3 cm^{-1}. Still, there is at least some hope that this band might be analytically useful. The remaining bands in these regions are too heavily overlapped, have insufficient frequency separation among the conformers, or have insufficient intensity to be of use in learning about individual conformers.

In the methyl stretching region (2850−3000 cm^{-1}) all vibrational modes between the conformers have nearly identical stretching frequencies and offer no possibility for spectral separation in a mixture.

Spectral Separation of the Conformers of *n*-Si_5Me_{12}. For studies of the optical properties, photophysics, and photochemistry of oligosilanes, it would be very desirable to examine the various conformers one at a time. There are various ways in which the individual conformers of *n*-Si_5Me_{12} might be spectrally observed and characterized separately. A procedure[49] that permitted a spectral resolution of the two conformers of *n*-C_4H_{10},[50] of all three confomers of *n*-C_4F_{10},[34] and of two of the three expected conformers of *n*-Si_4Me_{10}[12] is matrix trapping of a hot gaseous conformer mixture followed by various kinds of manipulation and spectral measurement. This takes advantage of the fact that the gas-phase conformer distribution tends to be trapped in the low-temperature matrix, since the cooling is fast relative to the rate of conformer interconversion.[51] Initial relative conformer abundances can thus be expected to be given more reliably by the MP2 (MM3) than the HF (MM2) results. However, changes in these abundances upon annealing should follow the HF (MM2) rather than MP2 (MM3) energies.

Resolving all eight (or nine) conformers of *n*-Si_5Me_{12} spectroscopically in this manner will prove to be very difficult for three reasons. (i) The structural differences of several of the conformers are too small to cause significant differences in their normal-mode frequencies. (ii) Those normal modes that show a large frequency variation among the conformers have weak calculated intensities. (iii) At temperatures at which *n*-Si_5Me_{12} can be expected to be stable, the abundance of the higher-energy conformations in the gas-phase conformer equilibrium is still rather low.

Nevertheless, it appears likely that a judicious combination of hot or cool vapor deposition, matrix annealing, and photodecomposition at selected wavelengths would allow the identification and separate spectral characterization of at least a few of the conformers.

Figures 11 and 12 show the two regions of the calculated vibrational spectra that offer the best opportunity for individual spectral separation of the conformers of *n*-Si_5Me_{12}, and Table 1 provides information on their predicted relative equilibrium abundances at various temperatures. The most promising region is 300−500 cm^{-1} in the Raman and 700−900 cm^{-1} in the IR spectrum.

We note first that the a_+g_+ and a_+g_- conformers have virtually identical predicted vibrational spectra and cannot be possibly distinguished by this type of experiment. Of the seven possibly distinguishable forms, we expect a_+a_+ to dominate the spectra of matrices deposited from vapor, and the singly twisted conformers a_+g_- and a_+g_+ to have comparable initial abundances, sufficient for detection. The spectrally indistinguishable last two conformers should convert into the first upon annealing. This transformation should be clearly apparent both in the IR (strong band near 815 cm^{-1}) and in the Raman (strong band near 340 cm^{-1}) spectra, and it is quite realistic to expect that the spectra of these forms can be derived by spectral subtractions. In higher temperature vapor depositions, the abundances

TABLE 7: Selected Calculated[a] Vibrational Frequencies of the Conformers of *n*-Si_5Me_{12}

	$\tilde{\nu}$ (cm^{-1})								I[b]	
mode	a_+a_+	a_+g_+	a_+g_-	a_+o_-	g_+g_+	g_+o_+	g_+o_-	o_+o_+	IR kcal mol^{-1}	Raman $Å^4$ amu^{-1}
SiCH def	813	817	818	818	820	820	820	820	391	0.05
asym SiSi str[c]	473	477	477	474	481	476	477	474	0.8	9.8
sym SiSi str[c]	429	431	430	429	438	433	436	431	1.2	8.8
asym SiSi str[d]	370	381	378	376	385	382	380	382	1.9	2.4
sym SiSi str[d]	353	340	340	345	329	334	334	337	1.2	35

[a] HF/3-21G* frequencies, scaled by 0.91. [b] Average calculated intensity. [c] Terminal SiSi bonds. [d] Internal SiSi bonds.

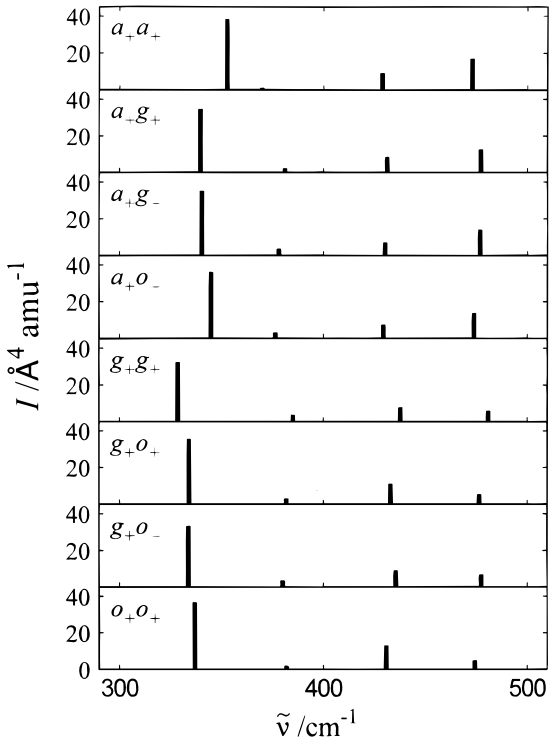

Figure 11. Low-frequency region of the Raman spectra calculated for the conformers of *n*-Si_5Me_{12} (HF/3-21G*, frequencies scaled by 0.91).

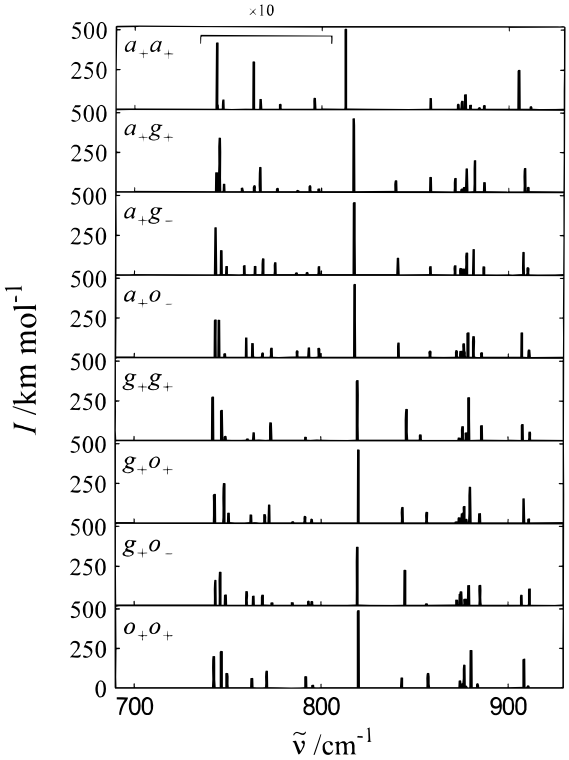

Figure 12. Low-frequency region of the IR spectra calculated for the conformers of *n*-Si_5Me_{12} (HF/3-21G*, frequencies scaled by 0.91).

of the a_+o_- and g_+g_+ conformers are likely to become sufficient for observation. There is slight hope that the former might be detected through its strong Raman band near 330 cm^{-1}, expected to lie between those of the a_+a_+ and a_+g_+ conformers, and it is quite likely that it will be possible to detect the latter through the analogous Raman band, now predicted to lie at significantly lower frequencies. We do not see much hope for the detection of the remaining three conformers g_+o_+, g_+o_-, and o_+o_+ by this technique.

Conclusions

In the present study we compared the computational results for the predicted conformers of *n*-Si_5Me_{12} at the HF and MM levels of calculation and found the relative energies computed at the MM+ and MM2 levels to be in close qualitative agreement with the HF energies at optimized geometries, whereas MM3 energies at optimized geometries resemble single-point MP2 energies at HF optimized geometries. Experimental information is sparse. Solution data seem to agree better with the HF results and gas-phase data with the MP2 results, and a rationalization has been proposed. Extrapolation from the SiSi bond conformations in *n*-Si_4Me_{10} yielded 12 possible unique conformational pairs, of which eight were found to correspond to potential energy minima and two to saddle points at the HF level of calculation. At the MM2 level and at the MM3 level,

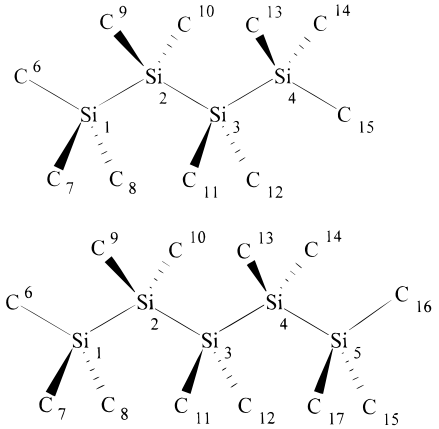

Figure 13. Atom numbering in *n*-Si_4Me_{10} and *n*-Si_5Me_{12} (Table 2).

six and nine conformational minima, respectively, were found. From the intrinsic bond conformation energies and two-bond conformation energies, extracted from calculations on *n*-Si_4Me_{10} and *n*-Si_5Me_{12}, respectively, a set of additive interaction increments were constructed at the MM2, MM3, HF, and MP2 (single point) levels of calculation. These simple additive models permit a prediction of the relative energies of longer-chain permethylated oligosilanes but need to be tested on longer chains before their use can be recommended. We found the relative

energies calculated at the MM3 level for several conformers of *n*-Si_6Me_{14} to be in general agreement with predictions using the MM3-based set of increments.

A comparison of the calculated (HF/3-21G*) vibrational spectra shows that for several of the eight conformers of *n*-Si_5Me_{12} the frequency differences in most or all of the individual normal modes are too small to be separately resolvable, or the calculated intensity is too weak to be detectable. Also, several conformers are expected to be present in amounts too small to be detectable. It appears that the method of hot vapor matrix deposition followed by annealing and/or irradiation, monitored by IR and Raman spectroscopy, will permit the identification of only about half of the expected conformers.

Acknowledgment. Work performed at the University of Colorado was supported by a grant from the USARO administered jointly with NSF/DMR (DAAH04-94-G-0018), by an NSF instrumentation grant (CHE 9709195), and by the Japan High Polymer Center within the framework of the Industrial Science and Technology Frontier Program funded by the New Energy and Industrial Technology Development Organization. B.A. acknowledges support by the Natural Science Research Council of Sweden. We are grateful to Prof. N. L. Allinger for supplying the values of MM3 parameters for silanes in advance of publication and also for allowing the use of his MM2 and MM3 programs and computers. We thank Dr. H. Teramae for performing single-point energy calculations on the conformers of *n*-Si_5Me_{12}.

Supporting Information Available: Figures 2, 9, and 10 showing calculated MM+ conformational energy contour map for *n*-Si_5Me_{12} and the full HF/3-21G* calculated IR and Raman spectra of the conformers of *n*-Si_5Me_{12} , respectively, and Table 6 listing calculated HF/3-21G* vibrational frequencies and IR and Raman intensities for the conformers of *n*-Si_5Me_{12}. This material is available free of charge via the Internet at http://pubs.acs.org.

References and Notes

(1) (a) Chalmers University of Technology. (b) University of Colorado.
(2) Miller, R. D.; Michl, J. *Chem. Rev.* **1989**, *89*, 1359.
(3) Gilman, H.; Atwell, W. H.; Schwebke, G. L. *Chem. Ind.* (*London*) **1964**, 1063. Gilman, H.; Atwell, W. H.; Schwebke, G. L. *J. Organomet. Chem.* **1964**, *2*, 369. Gilman, H.; Chapman, D. R. *J. Organomet. Chem.* **1966**, *5*, 392.
(4) Michl, J. *Acc. Chem. Res.* **1990**, *23*, 127.
(5) Yuan, C.-H.; West, R. *Macromolecules* **1998**, *31*, 1087. Gahimer, T.; Welsh, W. J. *Polymer* **1996**, *37*, 1815. West, R. In *Comprehensive Organometallic Chemistry II*; Abel, E. W., Stone, F. G. A., Wilkinson, G., Eds.; Pergamon: Oxford, 1995; Vol. 2, p 77. Obata, K.; Kira, M.; *RIKEN Rev.* **1995**, *11*, 39. Sanji, T.; Sakamoto, K.; Sakurai, H. *Bull. Chem. Soc. Jpn.* **1995**, *68*, 1052. Shukla, P.; Cotts, P. M.; Miller, R. D.; Russell, T. P.; Smith, B. A.; Wallraff, G. M.; Baier, M.; Thiyagarajan, P. *Macromolecules* **1991**, *24*, 5606. Miller, R. D.; Wallraff, G. M.; Baier, M.; Cotts, P. M.; Shukla, P.; Russell, T. P.; De Schryver, F. C.; Declercq, D. *J. Inorg. Organomet. Polym.* **1991**, *1*, 505. Harrah, L. A.; Zeigler, J. M. *J. Polym. Sci., Polym. Lett. Ed.* **1985**, *23*, 209. Trefonas, P., III; Damewood, J. R., Jr.; West, R.; Miller, R. D. *Organometallics* **1985**, *4*, 1318. Miller, R. D.; Hofer, D.; Rabolt, J.; Fickes, G. N. *J. Am. Chem. Soc.* **1985**, *107*, 2172.
(6) Miller, R. D.; Sooriyakumaran, R. *Macromolecules* **1988**, *21*, 3120. Oka, K.; Fujiue, N.; Dohmaru, T.; Yuan, C.-H.; West, R. *J. Am. Chem. Soc.* **1997**, *119*, 4074.
(7) Yuan, C.-H.; West, R. *Chem. Commun.* **1997**, 1825.
(8) Song, K.; Kuzmany, H.; Wallraff, G. M.; Miller, R. D.; Rabolt, J. F. *Macromolecules* **1990**, *23*, 3870.
(9) Fujino, M.; Hisaki, T.; Matsumoto, N. *Macromolecules* **1995**, *28*, 5017.
(10) Schweizer, K. S. *J. Chem. Phys.* **1986**, *85*, 1156, 1176. Fujiki, M. *J. Am. Chem. Soc.* **1996**, *118*, 7424. Bukalov, S. S.; Leites, L. A.; West, R.; Asuke, T. *Macromolecules* **1996**, *29*, 907.
(11) Albinsson, B.; Teramae, H.; Plitt, H. S.; Goss, L. M.; Schmidbaur, H.; Michl, J. *J. Phys. Chem.* **1996**, *100*, 8681.
(12) Albinsson, B.; Teramae, H.; Downing, J. W.; Michl, J. *Chem. Eur. J.* **1996**, *2*, 529.
(13) Takeda, K.; Matsumoto, N.; Fukuchi, M. *Phys. Rev. B* **1984**, *30*, 5871.
(14) Bock, H.; Ensslin, W.; Fehér, F.; Freund, R. *J. Am. Chem. Soc.* **1976**, *98*, 668. Damewood, J. R., Jr.; West, R. *Macromolecules* **1985**, *18*, 159. Bigelow, R. W.; McGrane, K. M. *J. Polym. Sci., Part B: Polym. Phys.* **1986**, *24*, 1233. Farmer, B. L.; Rabolt, J. F.; Miller, R. D. *Macromolecules* **1987**, *20*, 1167. Mintmire, J. W.; Ortiz, J. V. *Macromolecules* **1988**, *21*, 1189. Ortiz, J. V.; Mintmire, J. W. *J. Am. Chem. Soc.* **1988**, *110*, 4522. Mintmire, J. W. *Phys. Rev. B* **1989**, *39*, 13350. Teramae, H.; Takeda, K. *J. Am. Chem. Soc.* **1989**, *111*, 1281. Cui, C. X.; Karpfen, A.; Kertesz, M. *Macromolecules* **1990**, *23*, 3302. Jalali-Heravi, M.; McManus, S. P.; Zutaut, S. E.; McDonald, J. K. *Chem. Mater.* **1991**, *3*, 1024. Welsh, W. J. *Adv. Polym. Technol.* **1993**, *12*, 379. Ortiz, J. V.; McMichael Rohlfing, C. *Chem. Phys. Lett.* **1997**, *280*, 239. Obata, K.; Kabuto, C.; Kira, M. *J. Am. Chem. Soc.* **1997**, *119*, 11345.
(15) Welsh, W. J.; Johnson, W. D. *Macromolecules* **1990**, *23*, 1881.
(16) Welsh, W. J.; Debolt, L.; Mark, J. E. *Macromolecules* **1986**, *19*, 2978.
(17) Tachikawa, H. *Chem. Phys. Lett.* **1997**, *265*, 455. Yamaguchi, Y. *Int. J. Quantum Chem.* **1997**, *62*, 393.
(18) Sandorfy, C. *Can. J. Chem.* **1955**, *33*, 1337.
(19) Plitt, H. S.; Michl, J. *Chem. Phys. Lett.* **1992**, *198*, 400.
(20) Klingensmith, K. A.; Downing, J. W.; Miller, R. D.; Michl, J. *J. Am. Chem. Soc.* **1986**, *108*, 7438.
(21) Plitt, H. S.; Downing, J. W.; Raymond, M. K.; Balaji, V.; Michl, J. *J. Chem. Soc., Faraday Trans.* **1994**, *90* (12), 1653.
(22) Teramae, H.; Michl, J. *Mol. Cryst. Liq. Cryst.* **1994**, *256*, 149.
(23) Teramae, H.; Antic, D.; Crespo, R.; Michl, J. *Chem. Phys.*, in press.
(24) Imhof, R.; Antic, D.; David, D. E.; Michl, J. *J. Phys. Chem. A* **1997**, *101*, 4579.
(25) Imhof, R.; Teramae, H.; Michl, J. *Chem. Phys. Lett.* **1997**, *270*, 500.
(26) Mazières, S.; Raymond, M. K.; Raabe, G.; Prodi, A.; Michl, J. *J. Am. Chem. Soc.* **1997**, *119*, 6682.
(27) Ernst, C. A.; Allred, A. L.; Ratner, M. A. *J. Organomet. Chem.* **1979**, *178*, 119.
(28) Clementi, E.; Kistenmacher, H.; Popkie, H. *J. Chem. Phys.* **1973**, *58*, 4699. Payne, P. W.; Allen, L. C. In *Applications of Electronic Structure Theory*; Schaefer, H. F., III, Ed.; Plenum: New York, 1977; Vol. 4, p 29.
(29) Neumann, F.; Teramae, H.; Downing, J. W.; Michl, J. *J. Am. Chem. Soc.* **1998**, *120*, 573.
(30) Neumann, F.; Michl, J. Chain Conformations. In *Encyclopedia of Computational Chemistry*; Schleyer, P. v. R., Ed.; Wiley: Chichester, England, in press.
(31) Morokuma, K. L. *J. Chem. Phys.* **1971**, *54*, 962.
(32) Beckhaus, H.-D.; Rüchardt, C.; Anderson, J. E. *Tetrahedron* **1982**, *38*, 2299.
(33) Smith, G. D.; Jaffe, R. L.; Yoon, D. Y. *Macromolecules* **1994**, *27*, 3166.
(34) Albinsson, B.; Michl, J. *J. Am. Chem. Soc.* **1995**, *117*, 6378. Albinsson, B.; Michl, J. *J. Phys. Chem.* **1996**, *100*, 3418.
(35) Lambert, J. B.; Pflug, J. L.; Denari, J. M. *Organometallics* **1996**, *15*, 615.
(36) (a) Frisch, M. J.; Trucks, G. W.; Head-Gordon, M.; Gill, P. M. W.; Wong, M. W.; Foresman, J. B.; Johnson, B. G.; Schlegel, H. B.; Robb, M. A.; Replogle, E. S.; Gomperts, R.; Andres, J. L.; Raghavachari, K.; Binkley, J. S.; Gonzales, C.; Martin, R. L.; Fox, D. J.; DeFrees, D. J.; Baker, J.; Stewart, J. J. P.; Pople, J. A. *Gaussian 92*, revision C; Gaussian Inc.: Pittsburgh, PA, 1992. (b) Frisch, M. J.; Trucks, G. W.; Schlegel, H. B.; Gill, P. M. W.; Johnson, B. G.; Robb, M. A.; Cheeseman, J. R.; Keith, T. A.; Petersson, G. A.; Montgomery, J. A.; Raghavachari, K.; Al-Laham, M. A.; Zakrzewski, V. G.; Ortiz, J. V.; Foresman, J. B.; Cioslowski, J.; Stefanov, B. B.; Nanayakkara, A.; Chappacombe, M.; Peng, C. Y.; Ayala, P. A.; Wong, M. W.; Andres, J. L.; Replogle, E. S.; Gomperts, R.; Martin, R. L.; Fox, D. J.; Binkley, J. S.; DeFrees, D. J.; Baker, J.; Stewart, J. P.; Head-Gordon, M.; Gonzalez, C.; Pople, J. A. *Gaussian 94*, revision D.4; Gaussian Inc.: Pittsburgh, PA, 1995.
(37) Gordon, M. S.; Binkley, J. S.; Pople, J. A.; Pietro, W. J.; Hehre, W. J. *J. Am. Chem. Soc.* **1982**, *104*, 2797. Binkley, J. S.; Pople, J. A.; Hehre, W. J. *J. Am. Chem. Soc.* **1980**, *102*, 939. Pietro, W. J.; Francl, M. M.; Hehre, W. J.; DeFrees, D. J.; Pople, J. A.; Binkley, J. S. *J. Am. Chem. Soc.* **1982**, *104*, 5039. Dobbs, K. D.; Hehre, W. J. *J. Comput. Chem.* **1986,** *7*, 359. Dobbs, K. D.; Hehre, W. J. *J. Comput. Chem.* **1987**, *8*, 861. Dobbs, K. D.; Hehre, W. J. *J. Comput. Chem.* **1987**, *9*, 880.
(38) Hariharan, P. C.; Pople, J. A. *Theor. Chim. Acta* **1973**, *28*, 213. Hariharan, P. C.; Pople, J. A. *Mol. Phys.* **1974**, *27*, 209. Ditchfield, R.; Hehre, W. J.; Pople, J. A. *J. Chem. Phys.* **1971**, *54*, 724. Hehre, W. J.; Ditchfield, R.; Pople, J. A. *J. Chem. Phys.* **1972**, *56*, 2257. Gordon, M. S. *Chem. Phys. Lett.* **1980**, *76*, 163.
(39) Allinger, N. L. *J. Am. Chem. Soc.* **1977**, *99*, 8127. Frierson, M. R.; Imam, M. R.; Zalkow, V. B.; Allinger, N. L. *J. Org. Chem.* **1988**, *53*, 5248.

(40) *HyperChem*, version 4; Hypercube, Inc.: Gainesville, FL, 1996.
(41) Chen, K.; Allinger, N. L. *J. Phys. Org. Chem.* **1997**, *10*, 697.
(42) *Spartan*, version 4.0; Wavefunction, Inc.; Irvine, CA, 1995.
(43) Prof. Allinger allowed us the use of his computers to perform MM2 and MM3 force field calculations using his MM2(92) and MM3(96) programs.
(44) The MM2 program is available to nonprofit organizations from the Quantum Chemistry Program Exchange, University of Indiana, Bloomington, IN 47405.
(45) The MM3 program is available to all users from Tripos Associates, 1699 South Hanley Road, St. Louis, MO 63144, and to nonprofit organizations from the Quantum Chemistry Program Exchange, University of Indiana, Bloomington, IN 47405.
(46) Foresman, J. B.; Frisch, A. *Exploring Chemistry with Electronic Structure Methods*, 2nd ed.; Gaussian, Inc.: Pittsburgh, 1996, p 64.
(47) Allinger, N. L.; Yuh, Y. H.; Lii, J.-H. *J. Am. Chem. Soc.* **1989**, *111*, 8551. Lii, J.-H.; Allinger, N. L. *J. Am. Chem. Soc.* **1989**, *111*, 8576.
(48) Raymond, M. K. Ph.D. Dissertation, University of Colorado, Boulder, 1997. Raymond, M. K.; Michl, J. *Int. J. Quantum Chem.*, in press. Raymond, M. K.; Magnera, T. F.; Zharov, I.; West, R.; Dreczewski, B.; Nozik, A. J.; Sprague, J.; Ellingson, R. J.; Michl, J. In *Applied Fluorescence in Chemistry, Biology, and Medicine*; Rettig, W., Strehmel, B., Schrader, S., Eds.; Springer-Verlag: Heidelberg, in press.
(49) Huber-Wälchli, P.; Günthard, Hs. H. *Chem. Phys. Lett.* **1975**, *30*, 347.
(50) Rasanen, M.; Bondybey, V. E. *Chem. Phys. Lett.* **1984**, *111*, 515.
(51) *Vibrational Spectroscopy of Trapped Species: Infrared and Raman Studies of Matrix-Isolated Molecules, Radicals and Ions*; Hallam, H. E., Ed.; John Wiley & Sons: London, 1973.